

On the inclusion of cusp effects in expectation values with explicitly correlated Gaussians

Péter Jeszenszki,¹ Robbie T. Ireland,^{1,2} Dávid Ferenc,¹ and Edit Mátyus¹

¹*Institute of Chemistry, ELTE, Eötvös Loránd University,
Pázmány Péter sétány 1/A, Budapest, H-1117, Hungary*

²*School of Chemistry, University of Glasgow, University Avenue, G12 8QQ, Glasgow, United Kingdom*
(Dated: June 22, 2021)

This paper elaborates the integral transformation technique of [K. Pachucki, W. Cencek, and J. Komasa, *J. Chem. Phys.* 122, 184101 (2005)] and uses it for the case of the non-relativistic kinetic and Coulomb potential energy operators, as well as for the relativistic mass-velocity and Darwin terms. The techniques are tested for the ground electronic state of the helium atom and new results are reported for the ground electronic state of the H_3^+ molecular ion near its equilibrium structure.

I. INTRODUCTION

We wish to dedicate this paper to István Mayer’s memory. Two of us attended his undergraduate special course (called ‘speci’ among the students) at ELTE that he held until ca. 2010. During our everyday work, we still frequently point to simple calculations and theorems that we have learned from him and from his book [1]. As students, and later, as young researchers, we got to know him as an infinitely patient and supportive person towards the youths and their small things in research. His every reasoning and calculation was simple, because he made them simple and made every small step clear. In this spirit, we work out in detail the theoretical background for a nice technique proposed by Pachucki, Cencek, and Komasa that makes it possible to correct for the effects of the missing cusp of Gaussian basis functions during the evaluation of the ‘singular’ integrals in the Breit–Pauli Hamiltonian [2]. We imagine presenting this work on a research seminar: we can almost see István Mayer sitting and smiling in the first row of the auditorium and he has several comments and questions. We wonder: what are they?

Pachucki, Cencek, and Komasa [2] proposed the integral transformation technique to enhance the convergence of the expectation value of terms of the Breit–Pauli Hamiltonian that were known to be difficult to evaluate precisely in the commonly used explicitly correlated Gaussian (ECG) basis sets [3–6]

$$\Theta_i(\mathbf{r}) = \exp \left[-(\mathbf{r} - \mathbf{s}_i)^T \underline{\mathbf{A}}_i (\mathbf{r} - \mathbf{s}_i) \right], \quad (1)$$

where $\mathbf{r} \in \mathbb{R}^{3n}$ is the position vector of the particles, while $\mathbf{s}_i \in \mathbb{R}^{3n}$ and $\underline{\mathbf{A}}_i = \mathbf{A}_i \otimes 1^{[3]}$ with $\mathbf{A}_i \in \mathbb{R}^{n \times n}$ are parameters of the basis function. The parameterization is selected by minimization of the non-relativistic energy. The advantage of the ECG basis set is that it is an n -particle basis, for which analytic matrix elements can be derived for almost all physically relevant operators. At the same time, it is also well-known that the Gaussian functions fail to reproduce the analytic properties of the exact non-relativistic wave function at the particle-particle coalescence points (cusps) and in the asymptotic range for large particle-particle separations. The integral transformation technique offers a possibility to correct for the missing cusp effects.

We start the present work by writing out the theoretical background of Ref. [2] in detail. During this work, we have noticed that the ideas used for the ‘integral transform’ evaluation of the perturbative relativistic corrections may be more generally applicable. In a nutshell, instead of directly evaluating the expectation value of some physical quantity with the approximate wave function

$$\langle \hat{O} \rangle = \int d\mathbf{r}_1 \dots d\mathbf{r}_N \Psi(\mathbf{r}_1, \dots, \mathbf{r}_N)^* \hat{O} \Psi(\mathbf{r}_1, \dots, \mathbf{r}_N), \quad (2)$$

it becomes possible to incorporate the effects of the cusp of the exact wave function. An appropriate transformation is defined by introducing $\mathcal{I}_{\hat{O}}$ with variable ξ , and the integral is calculated in two parts,

$$\langle\langle \hat{O} \rangle\rangle = \int_0^{\xi_\Lambda} d\xi \mathcal{I}_{\hat{O}}(\xi) + \int_{\xi_\Lambda}^\infty d\xi \tilde{\mathcal{I}}_{\hat{O}}(\xi). \quad (3)$$

In the short-range part, $0 \leq \xi \leq \xi_\Lambda$, the cusp has a negligible effect and it can be accurately computed with an ECG basis. For the long-range part, $\xi_\Lambda < \xi < \infty$, the exact cusp condition can be incorporated in the asymptotic tail of the transformed function by considering the analytic behaviour of the wave function near the coalescence points.

In Sections II and III, we work out the theoretical background and the analytic form of the long-range integrand for two types of integral transforms. Section IV is about the implementation, technical details and observations.

Numerical results are presented for the relativistic calculations in Sec. V, for the non-relativistic calculations in Sec. VI, and the paper ends with a summary and conclusions (Sec. VII).

II. INTEGRAL TRANSFORM FOR THE COULOMB INTERACTION AND THE DIRAC DELTA OF THE COORDINATE

In this section, we will consider the inclusion of the cusp effect for spatial integrals of operators that can be related to the inverse of the particle-particle distance, $1/r$. So, let's first consider the relationship [7, 8]:

$$\frac{1}{r_i} = \frac{2}{\sqrt{\pi}} \int_0^\infty dt e^{-r_i^2 t^2} \quad (4)$$

that can be understood as an integral transform (we call it t -transform for short) generation of $1/r_i$. Furthermore, by using

$$-4\pi\delta(\mathbf{r}_i) = \Delta_{\mathbf{r}_i} \frac{1}{r_i}, \quad (5)$$

we can write, following Ref. [2],

$$\delta(\mathbf{r}_i) = -\frac{1}{2\pi^{3/2}} \int_0^\infty dt 2t^2(3 - 2t^2 r_i^2) e^{-r_i^2 t^2}. \quad (6)$$

So, both operators can be generated as a t -integral

$$F(r_i) = \int_0^\infty dt f(r_i, t) e^{-r_i^2 t^2}, \quad (7)$$

where

$$\text{for } F(r_i) = 1/r_i : \quad f(r_i, t) = 2/\sqrt{\pi}, \quad (8)$$

and

$$\text{for } F(r_i) = \delta(\mathbf{r}_i) : \quad f(r_i, t) = -\pi^{-3/2} t^2 (3 - 2t^2 r_i^2). \quad (9)$$

Then, by generalizing Pachucki, Komasa and Cencek's work for $\delta(\mathbf{r})$ [2], we re-write the expectation value for $F(r_i)$ as

$$\begin{aligned} \langle \Psi | F(r_i) | \Psi \rangle &= \int d\mathbf{r}_1 \dots d\mathbf{r}_N \psi(\mathbf{r}_1, \dots, \mathbf{r}_N)^* F(r_i) \psi(\mathbf{r}_1, \dots, \mathbf{r}_N) \\ &= \int d\mathbf{r}_1 \dots d\mathbf{r}_N \left[\int_0^\infty dt f(r_i, t) e^{-r_i^2 t^2} \right] |\psi(\mathbf{r}_1, \dots, \mathbf{r}_N)|^2 \\ &= \int_0^\infty dt \int d\mathbf{r}_1 \dots d\mathbf{r}_N f(r_i, t) e^{-r_i^2 t^2} |\psi(\mathbf{r}_1, \dots, \mathbf{r}_N)|^2 \\ &= \int_0^\infty dt \int d\mathbf{r}_i f(r_i, t) e^{-r_i^2 t^2} \rho(\mathbf{r}_i) \\ &= \int_0^\infty dt \mathcal{I}_{F(r_i)}(t), \end{aligned} \quad (10)$$

where we have defined the integral transform function for $F(r_i)$ as

$$\mathcal{I}_{F(r_i)}(t) = \int d\mathbf{r}_i f(r_i, t) e^{-r_i^2 t^2} \rho(\mathbf{r}_i) \quad (11)$$

and this integral can be written in an analytic form for 'any' polynomial $f(r_i, t)$ of r_i and t . In particular,

$$\text{for } F(r_i) = 1/r_i : \mathcal{I}_{1/r_i}(t) = \frac{2}{\sqrt{\pi}} \int d\mathbf{r}_i e^{-r_i^2 t^2} \rho(\mathbf{r}_i) \quad (12)$$

and

$$\text{for } F(r_i) = \delta(\mathbf{r}_i) : \mathcal{I}_{\delta(\mathbf{r}_i)}(t) = -\pi^{-\frac{3}{2}} \int d\mathbf{r}_i t^2 (3 - 2t^2 r_i^2) e^{-r_i^2 t^2} \rho(\mathbf{r}_i). \quad (13)$$

At first sight, it may seem strange that we introduce these complicated integral expressions, Eqs. (11)–(13). This is especially true for the integral of Dirac delta that could be immediately obtained from the density at the origin. But, it is difficult to calculate the density at this point, due to the cusp of the wave function. In numerical computations, $\rho(\mathbf{r}_i)$ is expanded in terms of a finite number of basis functions. The commonly used Gaussian functions are smooth everywhere and they miss the correct description of the cusp [5, 8, 9].

The integral transformation in Eq. (11) widens out the effect of the density to a finite interval due to the term $e^{-r_i^2 t^2}$ (for finite t values), and over this finite interval the density can be represented accurately with smooth functions. The original integral value is obtained by integration for $t \in [0, +\infty)$. For larger t values, the Gaussian in Eq. (11) gets narrower and makes the short-range contribution (cusp) more important to $\mathcal{I}_{F(\mathbf{r}_i)}(t)$.

In the following paragraphs, it will be shown that for large t values, the analytic form of the integrand can be deduced from analytic properties of the density near the cusp. To be able to incorporate these analytic results, the full integral is evaluated as the sum of a short-range, $t \in [0, t_\Lambda]$, and a long-range, $t \in [t_\Lambda, \infty)$, part:

$$\left\langle\left\langle \frac{1}{r_i} \right\rangle\right\rangle = \int_0^{t_\Lambda} \mathcal{I}_{1/r_i}(t_i) dt + \int_{t_\Lambda}^{\infty} \tilde{\mathcal{I}}_{1/r_i}(t_i) dt, \quad (14)$$

where we introduced the $\langle\langle \rangle\rangle$ notation to emphasize the difference from the standard expectation value labelled with $\langle \rangle$. The short-range part is evaluated by direct integration over the finite interval $t \in [0, t_\Lambda]$ (Appendix A). To calculate the long-range part including the cusp effects, the following considerations are necessary.

A. Derivation of the long-range part from the cusp condition

According to Kato's cusp condition [1, 8, 10], the following relations hold for the exact non-relativistic wave function (in Hartree atomic units) for the electron-nucleus and for the electron-electron coalescence points, respectively,

$$\lim_{r_{iA} \rightarrow 0} \left\langle \frac{\partial \Psi}{\partial r_{iA}} \right\rangle_{\vartheta, \varphi} = -Z_A \psi(r_{iA} = 0) \quad \text{and} \quad \lim_{r_{ij} \rightarrow 0} \left\langle \frac{\partial \langle \Psi \rangle_{\vartheta, \varphi}}{\partial r_{ij}} \right\rangle_{\vartheta, \varphi} = \frac{1}{2} \psi(r_{ij} = 0), \quad (15)$$

where $\langle \rangle_{\vartheta, \varphi}$ indicate averaging for the spherical angles and Z_A is the nuclear charge number. These conditions are valid only if the wave function does not have a node at the coalescence point, otherwise, higher derivatives must be considered for a good description of the wave function in this regime [11, 12]. The coalescence condition can be further elaborated by considering the effect of higher derivatives of the wave function [13, 14], which can be also affected by three-particle coalescence conditions [15, 16]. In this paper, we use the simplest, original conditions of Eq. (15) that give the following relations for the density function [17]

$$\lim_{r_{ia} \rightarrow 0} \frac{\partial \rho}{\partial r_{ia}} = -2Z_A \rho(r_{ia} = 0) \quad \text{and} \quad \lim_{r_{ij} \rightarrow 0} \frac{\partial \rho}{\partial r_{ij}} = \rho(r_{ij} = 0). \quad (16)$$

Then, we may consider the expansion of the particle density by the coalescence point taken as the origin (0):

$$\rho(r) = \rho(0) - 2Z\rho(0)r + \sum_{j=2}^m B_j r^j + \mathcal{O}(r^{m+1}), \quad (17)$$

where $Z = Z_A$ is the nuclear charge number for the electron-nucleus and $Z = -1/2$ for the electron-electron coalescence.

To obtain the asymptotic form of $\mathcal{I}_{F(\mathbf{r}_i)}$, labelled with $\tilde{\mathcal{I}}_{F(\mathbf{r}_i)}$ (where tilde refers to the fact that it is valid for the asymptotic range), we insert the density expansion, Eq. (17), in the definition of the integral transform function, Eq. (11) and integrate out the angular coordinates

for $t > t_\Lambda$:

$$\tilde{\mathcal{I}}_{F(\mathbf{r}_i)}(t) = 4\pi \int_0^\infty dr_i r_i^2 f(r_i, t) e^{-r_i^2 t^2} \left[\rho(0) - 2Z\rho(0)r_i + \sum_{j=2}^m B_j r_i^j + \mathcal{O}(r_i^{m+1}) \right], \quad (18)$$

where for practical reasons, we truncate the expansion at some ('any') m value. The one-dimensional integral for r_i can be evaluated. For $F(\mathbf{r}_i) = 1/r_i$ with $f(r, t) = 2\pi^{-1/2}$ in Eq. (4), we obtain the asymptotic form as

$$\text{for } t > t_\Lambda : \quad \tilde{\mathcal{I}}_{1/r_i}(t) = \frac{1}{t^3} \left(2\pi\rho(0) - 8\sqrt{\pi}Z\rho(0)\frac{1}{t} + \sum_{j=2}^m B_j^{[1/r_i]} \frac{1}{t^j} \right), \quad (19)$$

while for $F(\mathbf{r}_i) = \delta(\mathbf{r}_i)$, $f(r, t) = -t^2(3 - 2t^2r_i^2)\pi^{-3/2}$ in Eq. (6), we have

$$\text{for } t > t_\Lambda : \quad \tilde{\mathcal{I}}_{\delta(\mathbf{r}_i)}(t) = \frac{1}{t^2} \left(\frac{4Z\rho(0)}{\sqrt{\pi}} - \frac{2}{\sqrt{\pi}} \sum_{j=2}^m B_j^{[\delta(\mathbf{r}_i)]} \frac{1}{t^{j-1}} \right). \quad (20)$$

It is interesting to note that the asymptotic tail of the Coulomb interaction, Eq. (19), decays faster than that of the Dirac delta, Eq. (20), leading to a faster convergence in a finite basis representation.

Using Eqs. (19) and (20), the integral from t_Λ to ∞ is obtained in an analytic form as

$$\int_{t_\Lambda}^{\infty} \tilde{\mathcal{I}}_{1/r_i}(t) dt = \frac{1}{t_\Lambda^2} \left(\pi\rho(0) - \frac{8}{3}\sqrt{\pi}Z\rho(0)\frac{1}{t_\Lambda} + \sum_{j=2}^m \frac{B_j^{[1/r_i]}}{j+2} \frac{1}{t_\Lambda^j} \right), \quad (21)$$

$$\int_{t_\Lambda}^{\infty} \tilde{\mathcal{I}}_{\delta(\mathbf{r}_i)}(t) dt = \frac{1}{t_\Lambda} \left(\frac{4Z\rho(0)}{\sqrt{\pi}} - \frac{2}{\sqrt{\pi}} \sum_{j=2}^m \frac{B_j^{[\delta(\mathbf{r}_i)]}}{j} \frac{1}{t_\Lambda^{j-1}} \right). \quad (22)$$

Although both expressions contain the particle density at the coalescence point, $\rho(0) = \langle \Psi | \delta(\mathbf{r}_i) | \Psi \rangle$, that is inaccurately represented in a Gaussian basis, we can obtain its precise value by using:

$$\rho(r_i = 0) = \langle \delta(\mathbf{r}_i) \rangle = \int_0^{t_\Lambda} \mathcal{I}_{\delta(\mathbf{r}_i)}(t) dt + \int_{t_\Lambda}^{\infty} \tilde{\mathcal{I}}_{\delta(\mathbf{r}_i)}(t) dt \quad (23)$$

in an iterative procedure. First, the short-range integral (first term in the right hand side) is calculated by a one-dimensional quadrature (since this integrand is too complicated for an analytic calculation), while the B_j parameters in the long-range part are obtained by fitting the asymptotic part, Eq. (20), to data points. The dataset for the fit corresponds to 'intermediate'-range t values (for practical details, see Secs. V, VI, and Appendix D). Then, using $\rho(r_i = 0)$, obtained directly from numerical integration, the $\tilde{\mathcal{I}}_{\delta(\mathbf{r}_i)}(t)$ asymptotic function can be evaluated. In the last step, we calculate the integrals in Eq. (23) that results in an improved value for $\rho(r_i = 0)$ and an improved $\tilde{\mathcal{I}}_{\delta(\mathbf{r}_i)}(t)$ asymptotic form. The iteration converges in a few cycles as it was noted already in Ref. [2]. Once we have the precise value for $\rho(0)$, we can have a good representation for the asymptotic tail of the Coulomb interaction, $\tilde{\mathcal{I}}_{1/r_i}(t)$ in Eq. (19). Then, the integral value for the Coulomb interaction including also the cusp effect can be obtained as:

$$\left\langle \left\langle \frac{1}{r_i} \right\rangle \right\rangle = \int_0^{t_\Lambda} \mathcal{I}_{1/r_i}(t) dt + \int_{t_\Lambda}^{\infty} \tilde{\mathcal{I}}_{1/r_i}(t) dt. \quad (24)$$

III. FOURIER TRANSFORM FOR THE KINETIC ENERGY AND THE MASS-VELOCITY TERMS

To calculate integrals of momentum operators, it is convenient to switch to momentum space. The Fourier transform of an ECG preserves the mathematical form of the function, and we need to consider only the changes in the parameterization. So, the Fourier transform of the basis function in Eq. (1) is [2]

$$\bar{\psi}(\mathbf{p}) = |\mathbf{A}|^{-\frac{3}{2}} \exp [-(\mathbf{p} - \bar{\mathbf{s}})^T \bar{\mathbf{A}}(\mathbf{p} - \bar{\mathbf{s}}) + \bar{C}], \quad (25)$$

with $\bar{\mathbf{s}} = -2i\mathbf{s}\underline{\mathbf{A}}$, $\bar{\mathbf{A}} = \frac{1}{4}\mathbf{A}^{-1}$, and $\bar{C} = -\mathbf{s}^T \underline{\mathbf{A}}\mathbf{s}$. For the expectation value of the non-relativistic kinetic ($k = 2$) and for the mass-velocity ($k = 4$) operators, we have to evaluate

$$\begin{aligned} \langle \Psi | p_1^k | \Psi \rangle &= \int d\mathbf{p}_1 \dots d\mathbf{p}_n p_1^k |\bar{\Psi}(\mathbf{p}_1, \dots, \mathbf{p}_n)|^2 \\ &= \int d\mathbf{p}_1 p_1^k \bar{\rho}(\mathbf{p}_1) \\ &= 4\pi \int_0^\infty dp p^{k+2} \bar{\rho}(p) \\ &= \int_0^\infty dp \mathcal{I}_{p^k}(p), \end{aligned} \quad (26)$$

where the angular integration is calculated according to Eq. (A5). The explicit integrals for $k = 2$ (p^2) are evaluated in Eqs. (A6)–(A7), and the calculation can be carried out similarly for $k = 4$. It is interesting to note that the momentum density is spherically symmetric (second step in Eq. (26)), even if $\mathbf{s}_i \neq 0$. This observation is connected to the properties of the Fourier transform of the ECG, Eq. (25), in which any shift vector is purely imaginary.

Similarly to the t -transform (Sec. II), the cusp dominating the small-scale behavior in coordinate space is important for the long-range part in the inverse (now momentum) space. To be able to exploit the different characteristics for the two ranges (short and large), the integral is evaluated in two parts,

$$\langle \langle \Psi | p_1^k | \Psi \rangle \rangle = \int_0^{p_\Lambda} dp \mathcal{I}_{p^k}(p) + \int_{p_\Lambda}^\infty dp \tilde{\mathcal{I}}_{p^k}(p), \quad (27)$$

where the short-range part corresponds to the first term and is calculated from the ECG representation by direct integration up to some appropriate p_Λ threshold. The long-range part (second term) is determined by the cusp effects, and its analytic properties can be derived for the asymptotic tail. We will label this analytic asymptotic expression by $\tilde{\mathcal{I}}_{p^k}(p)$ that is derived in the forthcoming subsection.

A. The asymptotic tail of the momentum density

To show the connection of the short-range behaviour in coordinate space dominated by the particle-particle coalescence point(s) and the long-range behaviour in momentum space, we need to consider a common theorem from numerical analysis [18] which connects the smoothness of a function, $f(x)$, with the asymptotic behavior after Fourier transformation, $\tilde{f}(k) = \int f(x)e^{ikx}dx$. The smoothness of $f(x)$ is defined by the number of continuous derivatives. If $f(x)$ is infinitely differentiable, $f(x) \in C^\infty$, or in other words $f(x)$ is smooth, then $\tilde{f}(k)$ decays exponentially fast at large k values. If the n th derivative corresponds to a Dirac delta function, then the first $n - 2$ derivatives are continuous, $f(x) \in C^{n-2}$, and $\tilde{f}(k)$ decays polynomially with $1/k^n$ (Appendix B).

We use this theorem to determine the analytic form for the asymptotic tail of the momentum density function. The momentum density, $\bar{\rho}(\mathbf{p})$, can be calculated by a double Fourier transformation of the density matrix [19],

$$\bar{\rho}(\mathbf{p}) = \frac{1}{8\pi^3} \int e^{i\mathbf{p}(\mathbf{r}-\mathbf{r}')} \rho(\mathbf{r}', \mathbf{r}) d\mathbf{r} d\mathbf{r}', \quad (28)$$

$$\rho(\mathbf{r}', \mathbf{r}) = \int \Psi^*(\mathbf{r}', \mathbf{r}_2, \dots, \mathbf{r}_n) \Psi(\mathbf{r}, \mathbf{r}_2, \dots, \mathbf{r}_n) \prod_{i=2}^n d\mathbf{r}_i. \quad (29)$$

By substituting Eq. (29) into Eq. (28) and by exchanging the order of integration, we arrive at an alternative expression for the momentum density,

$$\bar{\rho}(\mathbf{p}) = \int \tilde{\Psi}^*(\mathbf{p}, \mathbf{r}_2, \dots, \mathbf{r}_n) \tilde{\Psi}(\mathbf{p}, \mathbf{r}_2, \dots, \mathbf{r}_n) \prod_{i=2}^n d\mathbf{r}_i, \quad (30)$$

$$\tilde{\Psi}(\mathbf{p}, \mathbf{r}_2, \dots, \mathbf{r}_n) = \frac{1}{\sqrt{8\pi^3}} \int e^{-i\mathbf{p}\mathbf{r}} \Psi(\mathbf{r}, \mathbf{r}_2, \dots, \mathbf{r}_n) d\mathbf{r}. \quad (31)$$

To describe the asymptotic tail in momentum space, it is sufficient to consider those regions of the wave function, for which the singularity occurs at higher derivatives (Appendix B). These regions are the points at the position of the nuclei and at the electron-electron coalescence points, where the exact wave function cusps.

Let us focus on a cusp at nucleus A located at \mathbf{R}_A . Then, the integral form of the cusp condition [11, 20] is

$$\text{for } \mathbf{r}_i \approx \mathbf{R}_A : \quad \Psi(\mathbf{r}_1, \mathbf{r}_2, \dots, \mathbf{r}_i, \dots, \mathbf{r}_n) \approx \left\{ 1 - [Z_A + f_A(\vartheta_i, \varphi_i)] \sqrt{(\mathbf{r}_i - \mathbf{R}_A)^2} \right\} \Phi_i(\mathbf{r}_1, \mathbf{r}_2, \dots, \mathbf{r}_i, \dots, \mathbf{r}_n), \quad (32)$$

where Z_A is the nuclear charge number, $f_A(\vartheta_i, \varphi_i)$ is an angular term, and $\Phi(\mathbf{r}_1, \dots, \mathbf{r}_n)$ is a continuous function at least up to its second derivative according to \mathbf{r}_i at \mathbf{R}_A for every particle i . The $f_A(\vartheta_i, \varphi_i)$ term accounts for the angular dependence of the wave function around the cusp (it is not generally spherically symmetric). A more specific form for $f_A(\vartheta_i, \varphi_i)$ can be derived if we expand the one-electron contribution of the wave function around the cusp with the eigenfunctions of the hydrogen atom [1, 11, 20]. As the leading contribution of the radial part is related to r^ℓ , where ℓ is the angular momentum quantum number, we can neglect all the $\ell \geq 2$ angular terms. Therefore, in order to describe the non-spherical angular dependence, it is sufficient to consider the linear combinations of the first-order spherical harmonics ($Y_{1m}(\vartheta, \varphi)$, $m = -1, 0, 1$). We can average over the spherical angles, similarly to Eq. (15), and then, the angular dependence disappears. It is interesting to point out that the angular dependence disappears also for the large-momentum tail that is shown in Appendix C.

In order to examine the non-smoothness of the cusp, let us consider $\nabla_i^4 \Psi$:

$$\nabla_i^4 \Psi = - \left(\nabla_i^4 Z_A \sqrt{(\mathbf{r}_i - \mathbf{R}_A)^2} \right) \Phi_i + \phi_i \quad (33)$$

where ϕ_i collects all other terms, and those remainder terms are smooth with respect to \mathbf{r}_i near \mathbf{R}_A . (The effect from the other cusps can be accounted for by summing up the contributions.) If ∇_i^4 acts on the cusp, a Dirac delta singularity appears,

$$-Z_A \nabla_i^4 \sqrt{(\mathbf{r}_i - \mathbf{R}_A)^2} = -Z_A \nabla_i^2 \frac{2}{\sqrt{(\mathbf{r}_i - \mathbf{R}_A)^2}} = 8\pi Z_A \delta(\mathbf{r}_i - \mathbf{R}_A). \quad (34)$$

For the fourth derivative, the integral in Eq. (31) can be evaluated using the properties of Dirac delta in Eq. (34), and thus, we obtain the leading-order contribution for large momentum,

$$\text{for } |\mathbf{p}_i| > p_\Lambda : \quad \tilde{\Psi}(\mathbf{r}_1, \dots, \mathbf{p}_i, \dots, \mathbf{r}_n) = \frac{\sqrt{8} Z_A}{\sqrt{\pi} p_i^4} \Psi(\mathbf{r}_1, \mathbf{r}_2, \dots, \mathbf{R}_A, \dots, \mathbf{r}_n) e^{-i\mathbf{p}_i \mathbf{R}_A} + \mathcal{O}(p_i^{-6}). \quad (35)$$

This short calculation demonstrates that it is indeed the cusp that determines the large-momentum behavior. In Eq. (35) the next leading order comes with p_i^{-6} , as in the short range only the differentiation of the odd powers leads to the Dirac delta singularity. This also means that in the asymptotic momentum tail expansion the p_i^{-5} term can be neglected, though further odd powers of $1/p_i$ are retained in the expansion due to higher-order singularities in the wave function [13–15].

To generalize the calculation to several nuclei and electrons, we consider the following Ansatz which includes the effect for all the cusps of the exact wave function of a many-particle system,

$$\begin{aligned} \Psi(\mathbf{r}_1, \mathbf{r}_2, \dots, \mathbf{r}_i, \dots, \mathbf{r}_n) = & \sum_{i=1}^n \left\{ 1 - \sum_A^N [Z_A + f_A(\vartheta_i, \varphi_i)] \sqrt{(\mathbf{r}_i - \mathbf{R}_A)^2} \right. \\ & \left. + \sum_{j \neq i}^n \left[\frac{1}{2} + g(\vartheta_{ij}, \varphi_{ij}) \right] \sqrt{(\mathbf{r}_i - \mathbf{r}_j)^2} \right\} \Phi_i(\mathbf{r}_1, \mathbf{r}_2, \dots, \mathbf{r}_i, \dots, \mathbf{r}_n), \quad (36) \end{aligned}$$

where $g(\vartheta_{ij}, \varphi_{ij})$ takes into account the angular dependence of the short-range electron-electron correlation, similarly to the $f_A(\vartheta_i, \varphi_i)$ term for the electron-nucleus cusp [11, 20]. The calculation of the large-momentum effect of the electron-electron coalescence can be carried out in a similar manner to the electron-nucleus case, Eqs. (32)–(35), after a coordinate transformation to the center-of-mass and relative motion coordinates including the \mathbf{r}_{ij} displacement vector. The same arguments apply for the electron-electron cusp as for the electron-nucleus case, with the only difference that the nuclear charge number is replaced with $Z_{ee} = -1/2$. Then, the asymptotic tail in momentum space for a many-electron-many-nucleus system is obtained as

$$\begin{aligned} \text{for } |\mathbf{p}_i| > p_\Lambda : \quad \tilde{\Psi}(\mathbf{r}_1, \dots, \mathbf{p}_i, \dots, \mathbf{r}_n) = & \frac{\sqrt{2}}{\sqrt{\pi} p_i^4} \left[2 \sum_A^N Z_A \Psi(\mathbf{r}_1, \mathbf{r}_2, \dots, \mathbf{R}_A, \dots, \mathbf{r}_n) e^{-i\mathbf{p}_i \mathbf{R}_A} \right. \\ & \left. - \sum_{j \neq i}^n \Psi(\mathbf{r}_1, \mathbf{r}_2, \dots, \mathbf{r}_j, \dots, \mathbf{r}_n) e^{-i\mathbf{p}_i \mathbf{r}_j} \right] + \mathcal{O}(p_i^{-6}). \quad (37) \end{aligned}$$

To obtain the asymptotic tail for the momentum density, we substitute Eq. (37) into Eq. (30),

for $|\mathbf{p}| > p_\Lambda$:

$$\begin{aligned} \bar{\rho}(\mathbf{p}) = \frac{2}{\pi p^8} & \left[4 \sum_{A=1}^N Z_A^2 \rho(\mathbf{R}_A) + 4 \sum_{A=1}^N \sum_{B \neq A}^N Z_A Z_B \cos[\mathbf{p}(\mathbf{R}_A - \mathbf{R}_B)] \rho(\mathbf{R}_A, \mathbf{R}_B) \right. \\ & \left. - 2(n-1) \sum_A Z_A \left(\int e^{i\mathbf{p}(\mathbf{r}_2 - \mathbf{R}_A)} \Psi^*(\mathbf{R}_A, \mathbf{r}_2, \dots, \mathbf{r}_n) \Psi(\mathbf{r}_2, \mathbf{r}_2, \dots, \mathbf{r}_n) \prod_{i=2}^n d\mathbf{r}_i + cc. \right) + \eta(0) \right] \\ & + \mathcal{O}(p^{-10}) . \end{aligned} \quad (38)$$

The notation $\eta(0)$ corresponds to the pair-correlation density at the coalescence point,

$$\eta(0) = (n-1) \int \Psi^*(\mathbf{r}_2, \mathbf{r}_2, \dots, \mathbf{r}_n) \Psi(\mathbf{r}_2, \mathbf{r}_2, \dots, \mathbf{r}_n) \prod_{i=2}^n d\mathbf{r}_i . \quad (39)$$

We note it can be shown by partial integration of the integral in Eq. (38) that it is related to $1/p^4$ for high momentum values, and thus, its contribution to the momentum density can be neglected, since it gives contribution only for the $1/p^{12}$ term.

Next, we can average the momentum density over the momentum orientations, *i.e.*, integrate out the angular dependence of the \mathbf{p} vector and divide by 4π , that reads for the second term in the square bracket of Eq. (38) as

$$\frac{1}{4\pi} \int_0^{2\pi} d\varphi \int_{-1}^1 d(\cos \vartheta) \cos[\mathbf{p}(\mathbf{R}_A - \mathbf{R}_B)] = \frac{1}{2} \int_{-1}^1 dc \cos(pR_{AB}c) = \frac{1}{pR_{AB}} \sin(pR_{AB}) , \quad (40)$$

and thus, we obtain the spherically averaged momentum density

$$\begin{aligned} \text{for } p > p_\Lambda : \quad \bar{\rho}(p) &= \frac{1}{4\pi} \int_0^{2\pi} d\varphi \int_{-1}^1 d\cos \vartheta \bar{\rho}(\mathbf{p}) \\ &= \frac{2}{\pi p^8} \left[4 \sum_{A=1}^N Z_A^2 \rho(\mathbf{R}_A) + 8 \sum_{A=1}^N \sum_{B \neq A}^N Z_A Z_B \frac{\sin(pR_{AB})}{pR_{AB}} \rho(\mathbf{R}_A, \mathbf{R}_B) - \eta(0) \right] + \mathcal{O}(p^{-10}) . \end{aligned} \quad (41)$$

B. Asymptotic tail of $\mathcal{I}_{p^k}(p)$ and its contribution to $\langle\langle \Psi | p_1^k | \Psi \rangle\rangle$

Using the derived large-momentum asymptotic tail of the momentum density, Eq. (41), we can calculate the asymptotic tail of $\mathcal{I}_{p^k}(p)$, Eqs. (26)–(27),

for $p > p_\Lambda$:

$$\begin{aligned} \tilde{\mathcal{I}}_{p^k}(p) &= 4\pi p^{k+2} \bar{\rho}(p) = \frac{8}{p^{6-k}} \left[4 \sum_{A=1}^N Z_A^2 \rho(\mathbf{R}_A) + 8 \sum_{A=1}^N \sum_{B \neq A}^N Z_A Z_B \frac{\sin(pR_{AB})}{pR_{AB}} \rho(\mathbf{R}_A, \mathbf{R}_B) - \eta(0) \right] \\ &+ \sum_{j=1}^m \frac{A_j}{p^{7-k+j}} + \mathcal{O}(p^{-8+k-m}) , \end{aligned} \quad (42)$$

where the A_j coefficients are determined by fitting and m is chosen to fix the number of additional terms considered in the expansion. In our calculations the typical value for m was between 4 and 7.

Using these expressions, the contribution from the large-momentum tail to $\langle\langle \Psi | p_1^k | \Psi \rangle\rangle$ in Eq. (27), can be calculated. In this paper, we focus on the $k=2$ and $k=4$ cases, for which the final expression is

$$\begin{aligned} \int_{p_\Lambda}^\infty dp \tilde{\mathcal{I}}_{p^k}(p) &= \frac{8}{(5-k)p_\Lambda^{5-k}} \left[4 \sum_{A=1}^N Z_A^2 \rho(\mathbf{R}_A) - \eta(0) \right] \\ &+ 64 \sum_{A=1}^N \sum_{B=1}^N Z_A Z_B \rho(\mathbf{R}_A, \mathbf{R}_B) G_k(p_\Lambda, R_{AB}) \\ &+ \sum_{j=0}^m \frac{A_j}{(6-k+j)p_\Lambda^{6-k+j}} + \mathcal{O}(p_\Lambda^{-7+k-m}) \end{aligned} \quad (43)$$

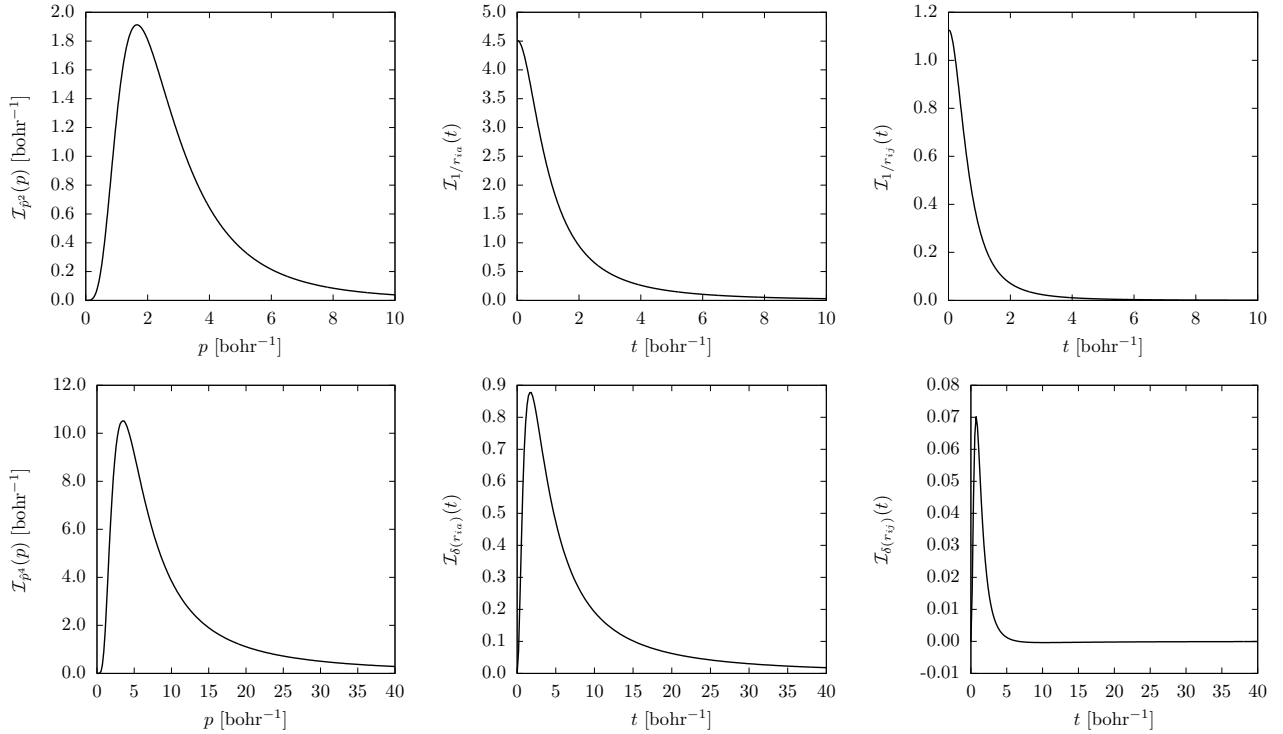


Figure 1. IT function profile for various operators, \mathcal{I}_{p^2} , $\mathcal{I}_{1/r_{ia}}$, $\mathcal{I}_{1/r_{ij}}$, \mathcal{I}_{p^4} , $\mathcal{I}_{\delta(r_{ia})}$, and $\mathcal{I}_{\delta(r_{ij})}$ for the example of the ground electronic state of the helium atom.

with

$$G_2(p_\Lambda, R) = \frac{\cos(Rp_\Lambda)}{2p_\Lambda} + \frac{\sin(Rp_\Lambda)}{2p_\Lambda^2 R} - \frac{R[\pi - 2\text{Si}(Rp_\Lambda)]}{4} \quad \text{for } k = 2, \quad (44)$$

$$G_4(p_\Lambda, R) = \frac{R^2 p_\Lambda^2 - 2}{24p_\Lambda^3} \cos(Rp_\Lambda) - \frac{R^2 p_\Lambda^2 - 6}{24Rp_\Lambda^4} \sin(Rp_\Lambda) + \frac{R^3[\pi - 2\text{Si}(Rp_\Lambda)]}{48} \quad \text{for } k = 2, \quad (45)$$

where $\text{Si}(x)$ is the sine integral function [21].

In the numerical calculations, $\rho(\mathbf{R}_A)$ and $\eta(0)$ are determined by using the method described in Sec. II,

$$\rho(\mathbf{R}_A) = \sum_{i=1}^n \langle \Psi | \delta(\mathbf{r}_i - \mathbf{R}_A) | \Psi \rangle, \quad (46)$$

$$\eta(0) = \sum_{i=1}^n \sum_{j>i}^n \langle \Psi | \delta(\mathbf{r}_i - \mathbf{r}_j) | \Psi \rangle. \quad (47)$$

$\rho(\mathbf{R}_A, \mathbf{R}_B)$ is a density matrix, for which the cusp condition is also known [22, 23], but it is handled as a fitting parameter in the present work.

IV. COMPUTATIONAL DETAILS

The integral transformed functions \mathcal{I}_{p^2} , \mathcal{I}_{p^4} , $\mathcal{I}_{1/r_{ia}}$, $\mathcal{I}_{1/r_{ij}}$, $\mathcal{I}_{\delta(r_{ia})}$, and $\mathcal{I}_{\delta(r_{ij})}$ are shown in Figures 1 and 2 for the example of the ground electronic state of the helium atom (He) and the tryhydrogen cation (H_3^+) with protons (p) clamped at an equilateral triangular configuration with $R_{pp} = 1.65$ bohr.

Up to a certain ξ_Λ value ($\xi_\Lambda = p_\Lambda$ for momentum operators, and $\xi_\Lambda = t_\Lambda$ for Coulombic operators), we calculate the short-range integral analytically for \mathcal{I}_{p^2} , $\mathcal{I}_{1/r_{ia}}$, $\mathcal{I}_{1/r_{ij}}$, and by quadrature for \mathcal{I}_{p^4} , $\mathcal{I}_{\delta(r_{ia})}$, and $\mathcal{I}_{\delta(r_{ij})}$ (for more details see Appendix A). For the long-range part, it is necessary to determine the accurate value of $\rho(0)$ and $\eta(0)$, which is calculated by an iterative procedure using Eqs. (20) and (23). Then, the long-range part is obtained by fitting the

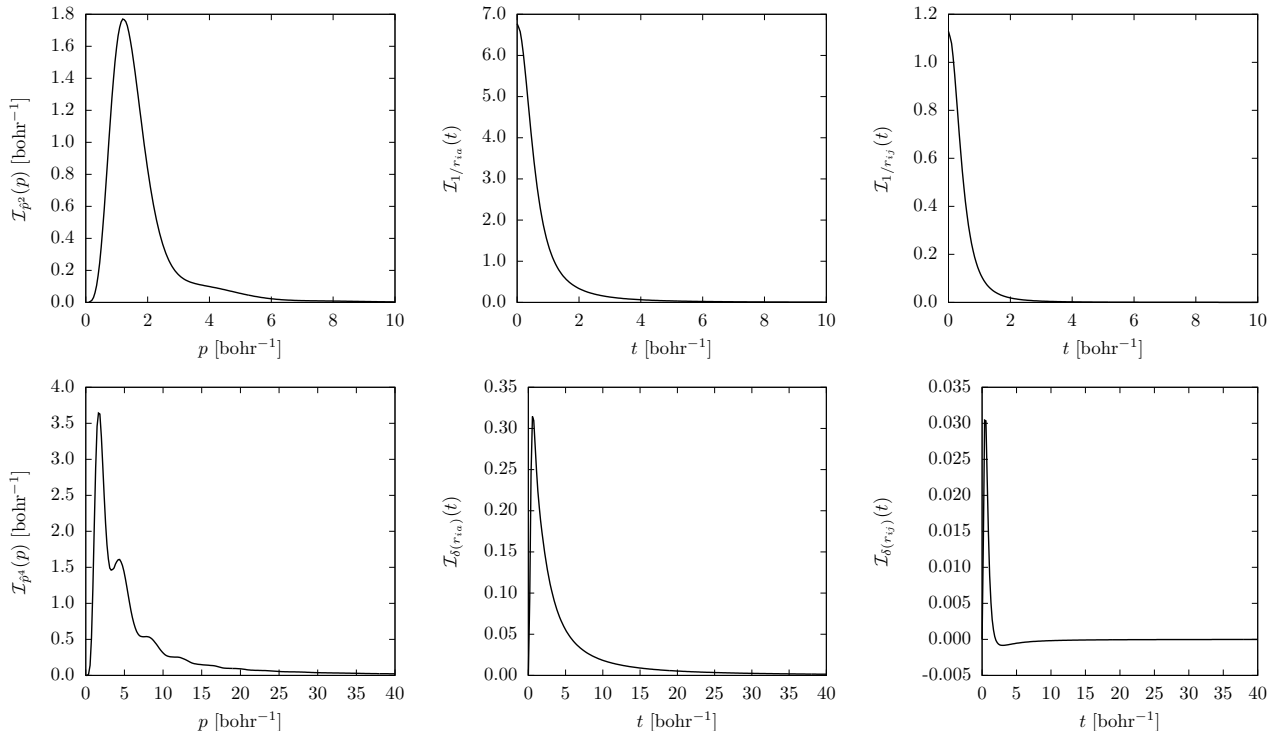


Figure 2. IT function profile for various operators, \mathcal{I}_{p^2} , $\mathcal{I}_{1/r_{ia}}$, $\mathcal{I}_{1/r_{ij}}$, \mathcal{I}_{p^4} , $\mathcal{I}_{\delta(r_{ia})}$, and $\mathcal{I}_{\delta(r_{ij})}$ for the example of the ground electronic state of the H_3^+ with protons (p) clamped at an equilateral triangular configuration with $R_{pp} = 1.65$ bohr.

asymptotic tail to data points using Eqs. (19) and (42) that is followed by the analytic integration of the asymptotic tail, Eqs. (21) and (43), using the fitted parameters.

It is critical to choose an optimal ξ_Λ value and a good interval for the data used for the fitting of the long-range analytic expression. We have selected these parameters based on the inspection of the integrand evaluated with the approximate wave function (Figs. 1 and 2). Close to the origin, the asymptotic expansion fails, but the ECG basis describes well the non-analytic correlation effects. For the spherically symmetric ground state of the helium atom (Fig. 1), $\mathcal{I}(\xi)$ is simple, it decreases monotonically to zero after an initial peak. The asymptotic part can be ‘easily’ identified and fitted to the asymptotic series. H_3^+ (Fig. 2) is a more ‘complex’ system, with more complicated correlation effects, and thus, we need to choose a larger ξ_Λ value to reach the asymptotic regime.

According to Secs. II A and III A, the long-range part of the function $\mathcal{I}(\xi)$ decays polynomially due to the cusp in the exact wave function that is approximated in the computations. At the same time, we may observe in Figure 3 that the approximate $\mathcal{I}_{p^k}(p)$ ($k = 2, 4$) function, corresponding to a finite ECG basis set, has artificial oscillations in momentum space and some non-negligible deviations in t -space. If the full integral is computed by direct integration, the oscillations approximately cancel in the integral, and this explains the practical observation that accurate results can be obtained even with ECGs that fail to satisfy analytic properties of the exact wave function. We aim to obtain more accurate integral values by replacing the oscillatory asymptotic tail with the mathematically correct decaying form corresponding to the cusp.

In practice, the numerical accuracy of the computations can be affected by the grids used for the numerical integration (if no analytic intervals are available over the finite, short range interval) and for the fitting procedure. Our computational strategies are explained in the following sections for physical operators considered in this work.

V. PERTURBATIVE RELATIVISTIC CORRECTION FOR H_3^+ AT EQUILIBRIUM

For the spectroscopic characterization of compounds of light elements, the leading-order relativistic correction has been traditionally calculated as the expectation value of the Breit–Pauli Hamiltonian with the non-relativistic wave function. The Breit–Pauli Hamiltonian is the the leading-order Foldy–Wouthusen perturbation theory (FWPT) term of the Dirac–Coulomb–Breit Hamiltonian [24–26]. The singular operators that are difficult to evaluate in a Gaussian basis appear already for the the leading-order FWPT of the Dirac–Coulomb (DC) operator that reads for the two

Table I. Expectation value of leading-order Foldy–Woythusen perturbative relativistic operators, in E_h , computed by direct integration (‘Direct’) and by the integral transformation technique (‘IT’) for the ground electronic state of H_3^+ with protons (p) clamped at an equilateral triangular configuration with $R_{pp} = 1.65$ bohr. The basis set size corresponds to the use of D_{3h} point-group symmetry in the computations.

N_b	$(1/8)\langle\nabla_1^4 + \nabla_2^4\rangle$		$(\pi/2)\sum_{i=1}^2\sum_{A=1}^3Z_A\langle\delta(\mathbf{r}_i - \mathbf{R}_A)\rangle$			$\pi\langle\delta(\mathbf{r}_1 - \mathbf{r}_2)\rangle$	
	Direct	IT	Direct	IT	Direct	IT	
150	15.428 820	15.469 909	1.086 786 273	1.089 641 891	0.018 430 054	0.018 340 790	
200	15.446 739	15.470 961	1.088 110 465	1.089 651 086	0.018 407 593	0.018 336 611	
300	15.455 982	15.469 863	1.088 821 792	1.089 654 339	0.018 368 291	0.018 335 079	
400	15.456 244	15.469 869	1.088 836 952	1.089 654 512	0.018 360 864	0.018 334 828	
500	15.456 360	15.470 052	1.088 843 368	1.089 654 577	0.018 358 011	0.018 334 777	
600	15.456 386	15.470 107	1.088 845 002	1.089 654 597	0.018 357 565	0.018 334 773	

electrons of H_3^+ with fixed protons as

$$\hat{H}_{PT} = \hat{H}_{\text{nonrel}} + \hat{H}_{\text{rel}} \quad (48)$$

$$\hat{H}_{\text{rel}} = \underbrace{-\frac{1}{8c^2}\sum_{i=1}^2\nabla_i^4}_{\text{mass-velocity}} + \underbrace{\frac{\pi}{2c^2}\sum_{i=1}^2\sum_{A=1}^3Z_A\delta(\mathbf{r}_i - \mathbf{R}_A) - \frac{\pi}{c^2}\delta(\mathbf{r}_1 - \mathbf{r}_2)}_{\text{Darwin}}, \quad (49)$$

where \hat{H}_{nonrel} is the non-relativistic Hamiltonian, and the \hat{H}_{rel} ‘relativistic correction’ is the sum of the mass-velocity and the Darwin terms (and c is the speed of light).

The mass-velocity and Darwin terms are evaluated using the IT technique for the example of a polyatomic molecule, H_3^+ near its equilibrium structure (Table I). Regarding the computational parameters, the $\xi_\Lambda = 100$ bohr $^{-1}$ threshold value was appropriate also in this system similarly to the He and H_2 computations reported in [2]. The short-range integrals for $\delta(\mathbf{r}_{12})$, $\delta\mathbf{r}_{iA}$ and p_i^4 were calculated by quadrature. To be able to use a sufficiently large number of points, without having to switch to quadruple precision arithmetics, the numerical integration was carried out over three subintervals, $[0, 1]$ bohr $^{-1}$, $[1, 10]$ bohr $^{-1}$, and $[10, 100]$ bohr $^{-1}$, using 25, 35, and 35 Gauss–Legendre quadrature points, respectively. The value of the integrand at each grid point is obtained by direct evaluation of the finite basis ECG integral (Appendix A). This setup was sufficient for a parts-per-billion (ppb) convergence of the short-range numerical integral value.

For fitting, the long-range tail, we have discarded the first 20 points from of integration grid (that correspond to a range dominated by non-trivial correlation effects, Fig. 2) and carried out the fitting for the remaining points. In each fit, six parameters were included, and the squared sum of residuals was on the order of 10^{-20} (a.u.) for $\delta(\mathbf{r}_{ij})$ and $\delta(\mathbf{r}_{iA})$ and 10^{-10} (a.u.) for the $p_1^4 + p_2^4$.

Table I collects the FWPT-DC relativistic corrections obtained with direct integration and by IT technique that reduces the relative error of the expectation value by ca. 2 orders of magnitude. The leading-order FWPT energy of the Dirac–Coulomb operator is compared with the ppb-converged variational four-component energy [27] in Table II. The 25 n E_h deviation of the direct expectation value for the FWPT correction reduces to 5 n E_h in comparison with the variational result. This small deviation is due to the error of the finite-order PT calculation. We also note that the variational Dirac–Coulomb procedure is not affected by the slow convergence problem of the singular operators.

VI. AN ATTEMPT TO IMPROVE THE NON-RELATIVISTIC ENERGY WITH THE INTEGRAL TRANSFORMATION TECHNIQUE

According to Sections II and III, the integral transformation technique can be used also for the expectation values of the non-relativistic operators, $\langle\hat{p}^2\rangle$, $\langle 1/r_{iA}\rangle$, and $\langle 1/r_{ij}\rangle$. Although, these expectation values converge (much) faster, than the singular relativistic operators, pinpointing their precise value would be useful to have an (even) better estimate of the complete basis limit. In this section, we report observations of some exploratory work for the $\langle\hat{p}^2\rangle$ operator and the ground state of the helium atom.

Thanks to the simplicity of the $\mathcal{I}_{\hat{p}^2}$, $\mathcal{I}_{1/\hat{r}_{iA}}$, and $\mathcal{I}_{1/\hat{r}_{ij}}$ integrands, short-range analytic integrals can be calculated (Appendix A). To fit the $\tilde{\mathcal{I}}_{\hat{O}}(\xi)$ asymptotic part, an equidistant grid was used. The start of the fitting interval was determined based on inspection of the integrand functions (Fig. 1). In the one hand, we wanted to choose large ξ values to avoid fitting to non-trivial correlation features, on the other hand, we wanted to choose a not too large

Table II. Non-relativistic and perturbative (E_{DC}^{P}) and variational (E_{DC}^{V}) relativistic electronic energies, in E_{h} , for the ground electronic state of H_3^+ with protons (p) clamped at an equilateral triangular configuration with $R_{\text{pp}} = 1.65$ bohr (see also caption to Table I).

N_{b}	E_{nonrel}	$E_{\text{DC}}^{\text{P}}(\text{Direct})^{\text{a}}$	$E_{\text{DC}}^{\text{P}}(\text{IT})^{\text{a}}$	E_{DC}^{V} [27]
150	-1.343 835 557	-1.343 850 435	-1.343 850 455	-1.343 850 149
200	-1.343 835 606	-1.343 850 488	-1.343 850 508	-1.343 850 507
300	-1.343 835 623	-1.343 850 501	-1.343 850 518	-1.343 850 524
400	-1.343 835 624	-1.343 850 502	-1.343 850 520	-1.343 850 526
500	-1.343 835 625	-1.343 850 502	-1.343 850 521	-1.343 850 527
600	-1.343 835 625	-1.343 850 502	-1.343 850 522	-1.343 850 527

^a The perturbative relativistic corrections, $c^{-2} \left[-\frac{1}{8} \sum_{i=1}^2 \langle \nabla_i^4 \rangle + \frac{\pi}{2} \sum_{i=1}^2 \sum_{A=1}^3 \langle \delta(\mathbf{r}_i - \mathbf{R}_A) \rangle - \pi \langle \delta(\mathbf{r}_1 - \mathbf{r}_2) \rangle \right]$, were computed by direct integration ('Direct') and by the integral transform ('IT') technique.

ξ value to avoid the finite basis error of the ECG set. A short summary about the calculation of the necessary $\rho(0)$ and $\eta(0)$ values is provided in Appendix D. Figure 3 shows the relative difference of $\mathcal{I}_{\hat{O}}(\xi)$ represented by the finite basis expansion and by the analytically known leading-order asymptotic part, $\tilde{\mathcal{I}}_{p^k}^0(p) = 128\pi\rho(0)/p^{2+k}$, $\tilde{\mathcal{I}}_{1/r_{ia}}^0(t) = t^{-3}(2\pi\rho(0) - 16\sqrt{\pi}\rho(0)t^{-1})$, $\tilde{\mathcal{I}}_{1/r_{ij}}^0(t) = t^{-3}(2\pi\eta(0) + 4\sqrt{\pi}\eta(0)t^{-1})$. For larger ξ values (but not too large, *i.e.*, for which the finite basis representation can be trusted), the relative difference is determined by the contributions beyond the analytic, leading-order terms. The deviation from zero in the asymptotic limit indicates numerical errors, which originate from the finite basis-set approximation.

For the Coulomb terms, $\tilde{\mathcal{I}}_{1/r_{ij}}$ and $\tilde{\mathcal{I}}_{1/r_{ia}}$ (Figs. 3c, d), this numerical error is monotonic and has non-negligible values beyond some t value, but by increasing the basis set size, this critical t threshold is shifted towards larger values.

Regarding the \hat{p}^k operators (Figs. 3a, b), the Fourier transformation results in oscillations that can be observed for the finite-basis representation of $\mathcal{I}_{\hat{p}^k}$ over the large momentum range. The oscillation amplitude decreases upon increasing the basis set size. Figure 4 shows the comparison of the direct and the IT integration procedures for \hat{p}^2 and \hat{p}^4 . The computational details for \hat{p}^4 can be found in the Sec. IV. Regarding \hat{p}^2 , the fit is performed over the $[10, 90]$ bohr $^{-1}$ interval using 1600 equidistant points. Depending on the number of the fitting parameters the squared sum of the residuals varies between 10^{-11} and 10^{-17} (a.u.).

The effect of the choice of the p_{Λ} threshold value, which separates the short and long-range intervals, and the number of the fitted parameters in long-range part is shown in Figure 4. For both \hat{p}^2 and \hat{p}^4 , the larger the number of fitted parameters, the better results are observed, especially for smaller p_{Λ} values. By increasing p_{Λ} , all curves come close, since the high-order inverse momentum terms have a numerically negligible contribution in this regime. For $p_{\Lambda} \rightarrow \infty$, the contribution from integral transformation goes to zero, and the direct integration result is recovered. It is also necessary to note that although we achieve a better relative accuracy for $\langle\langle \hat{p}^2 \rangle\rangle$, than for $\langle\langle \hat{p}^4 \rangle\rangle$, the improvement of $\langle\langle \hat{p}^2 \rangle\rangle$ (IT) over $\langle\hat{p}^2\rangle$ ('direct') is modest. This observation can be contrasted with the two-orders of magnitude improvement of $\langle\langle \hat{p}^4 \rangle\rangle$ (IT) over $\langle\hat{p}^4\rangle$ ('direct') that appears to be a robust feature with respect to the choice of p_{Λ} and the fitting details. For \hat{p}^2 , the 'optimal' interval for p_{Λ} and the fitting details should be very carefully chosen to observe any improvement.

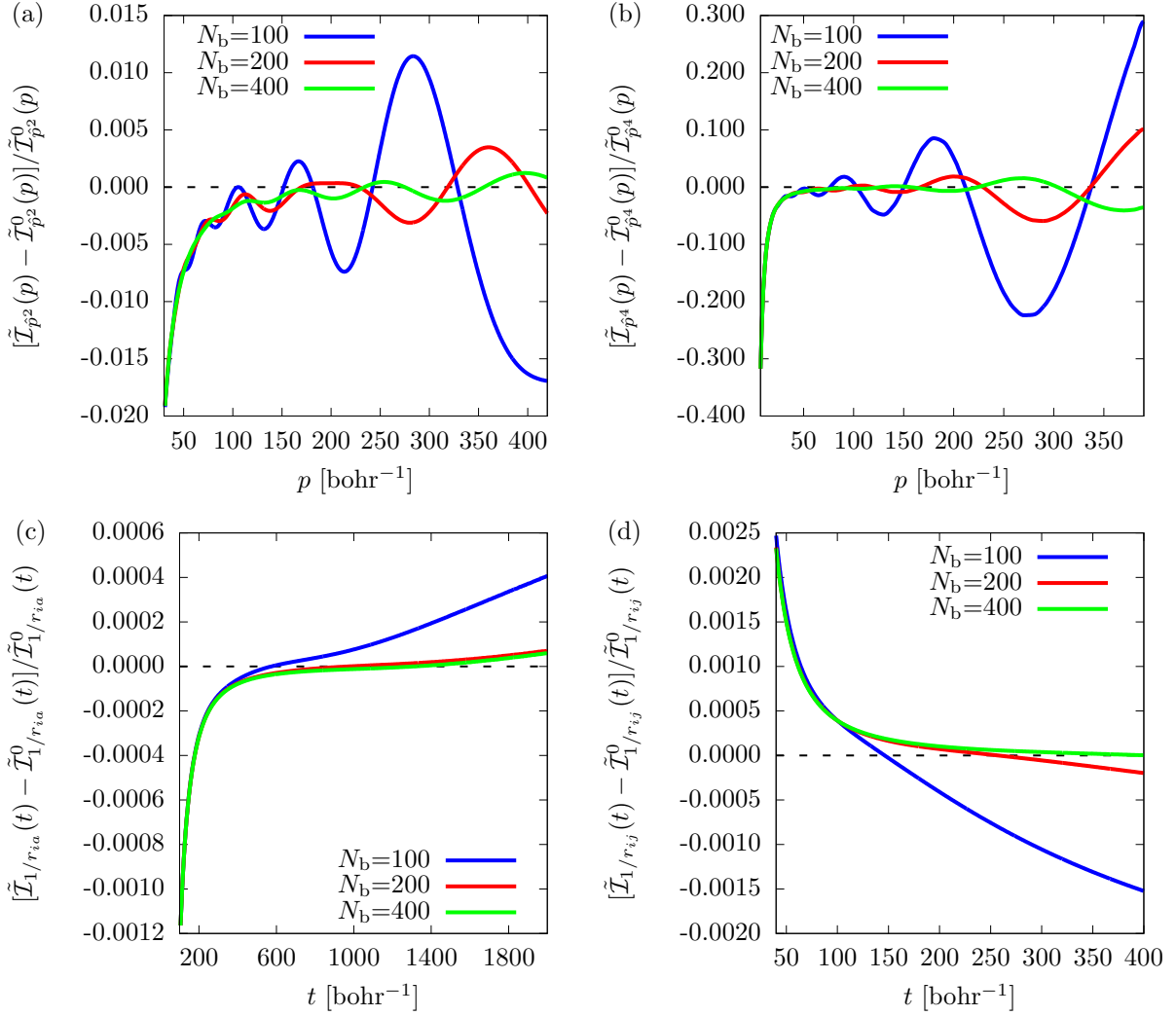


Figure 3. Relative difference in the asymptotic tail of the numerically calculated functions $\mathcal{I}_{p^2}(p)$, $\mathcal{I}_{p^4}(t)$, $\mathcal{I}_{1/r_{ia}}(t)$, $\mathcal{I}_{1/r_{ij}}(t)$, and the analytic leading order expressions of the asymptotic tail, $\tilde{\mathcal{I}}_{p^k}^0(p) = 128\pi\rho(0)/p^{2+k}$, $\tilde{\mathcal{I}}_{1/r_{ia}}^0(t) = t^{-3}(2\pi\rho(0) - 16\sqrt{\pi}\rho(0)t^{-1})$, $\tilde{\mathcal{I}}_{1/r_{ij}}^0(t) = t^{-3}(2\pi\eta(0) + 4\sqrt{\pi}\eta(0)t^{-1})$ for the example of the ground state of the helium atom with an increasing number of ECG basis functions (N_b).

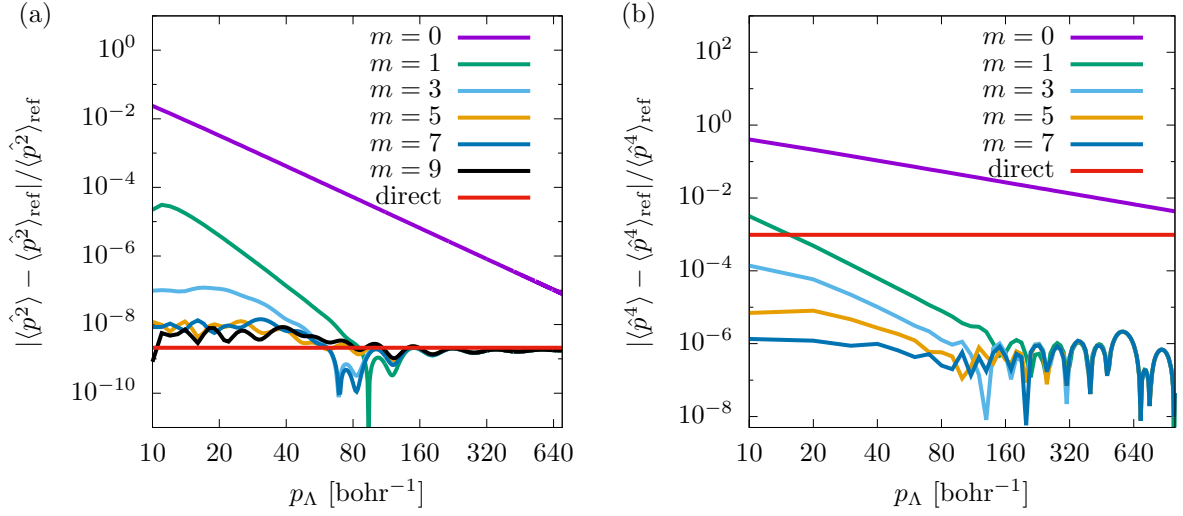


Figure 4. The relative error of $\langle \hat{p}^2 \rangle$ and $\langle \hat{p}^4 \rangle$ for various p_Λ thresholds, m number of fitting parameters in Eq. (43). The result ‘direct’ was obtained by direct integration with ECGs. $\langle \hat{p}^2 \rangle_{\text{ref}} = 2.9037243770341195$ bohr⁻² [28] (using the virial theorem $\langle \hat{T} \rangle = -E$). $\langle \hat{p}^4 \rangle_{\text{ref}} = 108.1761344(8)$ bohr⁻⁴ [2].

VII. SUMMARY AND CONCLUSION

Explicitly correlated Gaussian (ECG) functions are often used in atomic and molecular computations, because they incorporate particle-particle correlation and they have analytic integrals for most physically relevant operators. In spite of their advantages, they also have some drawbacks. They fail to describe correctly the particle coalescence points and the asymptotic tail of the exact non-relativistic wave function of Coulomb-interacting point-like particles. This paper was devoted to the study of a possible correction scheme for coalescence properties during computations with Gaussian-type functions.

For this purpose, we have presented the detailed theoretical background of the integral transformation (IT) technique originally proposed by Pachucki, Cencek, and Komasa [2] to enhance the convergence of singular operators appearing in perturbative relativistic corrections. The core idea of the IT technique is to rewrite expectation values of physical quantities with an approximate wave function into a form, for which the cusp effect—characteristic for short ranges in coordinate space—appears in the asymptotic tail of the integrand in an ‘inverse space’ (ξ). For momentum-type operators this transformation is the Fourier transformation and the inverse space is momentum space ($\xi = p$). For Coulomb-type operators this is a ‘ t -transformation’ (for which we are not aware of any common name), and for which the variable in the inverse space was labelled with $\xi = t$. Expectation values that contain the cusp effects are obtained by computing the integral as the sum of a short-, $0 \leq \xi < \xi_\Lambda$, and a long-range, $\xi_\Lambda \leq \xi < \infty$, part. The short-range part is calculated by direct integration with the approximate wave function expressed with ECGs.

We explained in this paper that the effect of the singular derivative of the wave function at the coalescence points, where the exact wave function cusps, appears in the asymptotic tail of the integrand in the inverse space. Using this connection and the analytic cusp conditions, we derived the analytic form of the long-range tail of the integrands for the p_i^2 , $1/r_{ij}$, $1/r_{iA}$ -type operators and our derivation reproduces the asymptotic expressions for p_i^4 , $\delta(r_{iA})$, and $\delta(r_{ij})$ of Ref. [2]. It is interesting to note that the asymptotic tail of the non-relativistic operators (p^2 and $1/r$) decay faster ($\sim 1/p^4$ and $\sim 1/t^3$), than the more ‘singular’ operators, \hat{p}^4 and $\hat{\delta}(\mathbf{r})$, $\sim 1/p^2$ and $\sim 1/t^2$, respectively.

Exploratory results were reported for the expectation values of the non-relativistic energy operators, for which, in principle, it should be possible to improve upon the non-relativistic energy with the inclusion of the cusp ‘effect’. The practical realization of this idea, appears to be limited, for the moment, by particular details of the fitting procedure of the asymptotic tail.

We also use the IT technique in this work to compute perturbative relativistic corrections for H_3^+ near its equilibrium structure. The leading-order perturbative relativistic energy is compared with the variational relativistic result of Ref. [27].

Finally, we would like to mention that the \hat{p}^4 - and $\delta(\mathbf{r})$ -type singular operators appear not only in the perturbative relativistic theory, but also in lower-bound theory due to the appearance of the \hat{H}^2 operator [5, 29–31]. This fact contributes to the observation that the energy lower bounds typically converge slower to the exact energy [5, 31], than the energy upper bound. It would be interesting to use (generalize) the IT technique to the \hat{H}^2 expectation value and variance computations, which may speed up the convergence of the best energy lower bounds [32] and that would open the route to computation of rigorous theoretical error bars for numerically computed non-relativistic energies.

ACKNOWLEDGMENTS

The authors thank Gustavo Avila for discussions about the quadrature integration. Financial support of the European Research Council through a Starting Grant (No. 851421) is gratefully acknowledged. RI thanks the Erasmus+ program for funding a traineeship at ELTE.

-
- [1] I. Mayer, *Simple Theorems, Proofs, and Derivations in Quantum Chemistry*, edited by P. G. Mezey, Mathematical and Computational Chemistry (Springer US, Boston, MA, 2003).
 - [2] K. Pachucki, W. Cencek, and J. Komasa, On the acceleration of the convergence of singular operators in Gaussian basis sets, *J. Chem. Phys.* **122**, 184101 (2005).
 - [3] B. Jeziorski and K. Szalewicz, High-accuracy Compton profile of molecular hydrogen from explicitly correlated Gaussian wave function, *Phys. Rev. A* **19**, 2360 (1979).
 - [4] W. Cencek and J. Rychlewski, Many-electron explicitly correlated Gaussian functions. I. General theory and test results, *J. Chem. Phys.* **98**, 1252 (1993).
 - [5] Y. Suzuki and K. Varga, *Stochastic Variational Approach to Quantum-Mechanical Few-Body Problems* (Springer, 1998).

- [6] J. Mitroy, S. Bubin, W. Horiuchi, Y. Suzuki, L. Adamowicz, W. Cencek, K. Szalewicz, J. Komasa, D. Blume, and K. Varga, Theory and application of explicitly correlated Gaussians, *Rev. Mod. Phys.* **85**, 693 (2013).
- [7] S. F. Boys, Electronic wave functions - I. A general method of calculation for the stationary states of any molecular system, *Proc. R. Soc. Lond. A* **200**, 542 (1950).
- [8] T. Helgaker, P. Jørgensen, and J. Olsen, *Molecular Electronic-Structure Theory* (John Wiley & Sons, Chichester, 2008).
- [9] C. Hättig, W. Klopper, A. Köhn, and D. P. Tew, Explicitly correlated electrons in molecules, *Chem. Rev.* **112**, 4 (2012).
- [10] T. Kato, On the eigenfunctions of many-particle systems in quantum mechanics, *Commun. Pure Appl. Math.* **10**, 151 (1957).
- [11] R. T. Pack and W. B. Brown, Cusp conditions for molecular wavefunctions, *J. Chem. Phys.* **45**, 556 (1966).
- [12] W. Kutzelnigg, Theory of the expansion of wave functions in a gaussian basis, *Int. J. Quantum Chem.* **51**, 447 (1994).
- [13] V. A. Rassolov and D. M. Chipman, Behavior of electronic wave functions near cusps, *J. Chem. Phys.* **104**, 9908 (1996).
- [14] D. P. Tew, Second order coalescence conditions of molecular wave functions, *J. Chem. Phys.* **129**, 014104 (2008).
- [15] S. Fournais, M. Hoffmann-Ostenhof, T. Hoffmann-Ostenhof, and T. O. Sorensen, Sharp regularity results for Coulombic many-electron wave functions, *Commun. Math. Phys.* **255**, 183 (2005).
- [16] C. R. Myers, C. J. Umrigar, J. P. Sethna, and J. D. Morgan, Fock's expansion, Kato's cusp conditions, and the exponential ansatz, *Phys. Rev. A* **44**, 5537 (1991).
- [17] E. Steiner, Charge densities in atoms, *J. Chem. Phys.* **39**, 2365 (1963).
- [18] B. Mercier, *An Introduction to the Numerical Analysis of Spectral Methods* (Springer Berlin, Berlin, 2014).
- [19] J. C. Kimball, Short-range correlations and the structure factor and momentum distribution of electrons, *J. Phys. A: Math. Gen.* **8**, 1513 (1975).
- [20] W. A. Bingel, The behaviour of the first-order density matrix at the Coulomb singularities of the Schrödinger equation, *Z. Naturforsch.* **18a**, 1249 (1963).
- [21] F. W. J. Olver, A. B. Olde Daalhuis, D. W. Lozier, B. I. Schneider, R. F. Boisvert, C. W. Clark, B. R. Miller, B. V. Saunders, H. S. Cohl, and M. A. McClain, *NIST Digital Library of Mathematical Functions: Sine and Cosine Integrals* (2021).
- [22] W. L. Clinton and L. J. Massa, The cusp condition: Constraint on the electron density matrix, *Int. J. Quantum Chem.* **6**, 519 (1972).
- [23] E. Davidson, *Reduced Density Matrices in Quantum Chemistry*. (Elsevier Science, Saint Louis, 2014).
- [24] K. G. Dyall and K. Fægri, *Introduction to Relativistic Quantum Chemistry* (Oxford University Press, New York, 2007).
- [25] M. Reiher and A. Wolf, *Relativistic Quantum Chemistry: The Fundamental Theory of Molecular Science*, 2nd ed. (Wiley-VCH, Weinheim, 2015).
- [26] W. Cencek and W. Kutzelnigg, Accurate relativistic energies of one- and two-electron systems using Gaussian wave functions, *J. Chem. Phys.* **105**, 5878 (1996).
- [27] P. Jezszowski, D. Ferenc, and E. Mátyus, All-order explicitly correlated relativistic computations for atoms and molecules, *J. Chem. Phys.* **154**, 224110 (2021).
- [28] G. Drake, High Precision Calculations for Helium, in *Springer Handbook of Atomic, Molecular, and Optical Physics*, edited by G. Drake (Springer New York, New York, NY, 2006) pp. 199–219.
- [29] D. H. Weinstein, Modified Ritz method, *Proc. Natl. Acad. Sci. U.S.A.* **20**, 529 (1934).
- [30] G. Temple, The theory of Rayleigh's principle as applied to continuous systems, *Proc. R. Soc. Lond. A* **119**, 276 (1928).
- [31] R. T. Ireland, P. Jezszowski, E. Mátyus, R. Martinazzo, M. Ronto, and E. Pollak, Lower bounds for atomic energies, in preparation (2021).
- [32] E. Pollak and R. Martinazzo, Lower bounds for Coulombic systems, *J. Chem. Theory Comput.* **17**, 1535 (2021).
- [33] E. Mátyus and M. Reiher, Molecular structure calculations: A unified quantum mechanical description of electrons and nuclei using explicitly correlated Gaussian functions and the global vector representation, *J. Chem. Phys.* **137**, 024104 (2012).
- [34] A discontinuous function cannot be differentiated in a rigorous way. However, the differentiation can be generalized using the so-called weak derivative [?], which can be calculated for these functions. This leads to the expected Dirac delta function as the weak derivative of the Heaviside step function.
- [35] F. W. J. Olver, A. B. Olde Daalhuis, D. W. Lozier, B. I. Schneider, R. F. Boisvert, C. W. Clark, B. R. Miller, B. V. Saunders, H. S. Cohl, and M. A. McClain, *NIST Digital Library of Mathematical Functions: Expansion of plane wave in spherical harmonics* (2021).
- [36] F. W. J. Olver, A. B. Olde Daalhuis, D. W. Lozier, B. I. Schneider, R. F. Boisvert, C. W. Clark, B. R. Miller, B. V. Saunders, H. S. Cohl, and M. A. McClain, *NIST Digital Library of Mathematical Functions: Spherical Bessel functions* (2021).
- [37] P. Uginčius, An integral representation for the Dirac delta function, *Am. J. Phys.* **40**, 1690 (1972).

Appendix A: Necessary Gaussian integrals for the short-range part

The approximate wave function is written as a linear combination of antisymmetrized products of χ spin and Θ ECGs functions,

$$\Psi = \sum_{I=1}^{N_b} c_I \hat{\mathcal{A}}\{\chi_I \Theta_I\} \quad (\text{A1})$$

with the $\hat{\mathcal{A}} = (N_{\text{perm}})^{-\frac{1}{2}} \sum_{p=1}^{N_{\text{perm}}} \varepsilon_p \hat{P}_p$ antisymmetrization operator over the N_{perm} possible permutations with ε_p parity. Expectation values of a (permutationally invariant) \hat{O} operator can be calculated as

$$\langle \Psi | \hat{O} | \Psi \rangle = \sum_{I=1}^{N_b} \sum_{J=1}^{N_b} \sum_{p=1}^{N_{\text{perm}}} c_I^* c_J \varepsilon_{IJp} \langle \Theta_I | \hat{O} | \Theta_{Jp} \rangle \quad (\text{A2})$$

where ε_{IJp} contains the parity of the permutation and the spin integrals, and we need to calculate matrix elements of \hat{O} with the ECG functions Θ_I and Θ_{Jp} . Particle permutation leaves the mathematical form of the ECG unchanged, and assumes transformation of the \mathbf{A} and \mathbf{s} parameter arrays (for further details, see for example, Ref. [33]).

During the IT procedure, the short-range part of the expectation values are computed by direct integration with the basis functions. For the short-range calculations, the following integrals were used.

1. Coulomb integral over the short-range interval

$$\begin{aligned} \left\langle \Theta_i \left| \left(\frac{1}{r} \right)_{\Lambda} \right| \Theta_j \right\rangle &= \frac{2}{\sqrt{\pi}} \int_0^{\Lambda} dt \left\langle \Theta_i \left| e^{-r_i^2 t^2} \right| \Theta_j \right\rangle \\ &= \frac{2}{\sqrt{\pi}} S_{ij} \int_0^{\Lambda} dt (1+t^2 a)^{-3/2} e^{-\frac{\beta t^2}{1+t^2 a}} \\ &= \frac{S_{ij}}{\sqrt{\pi \beta}} \int_0^{\frac{\Lambda^2 \beta}{1+\Lambda^2 a}} dz z^{-\frac{1}{2}} e^{-z} = \frac{S_{ij}}{\sqrt{\beta}} \operatorname{erf} \left[\left(\frac{\Lambda^2 \beta}{1+\Lambda^2 a} \right)^{\frac{1}{2}} \right] \end{aligned} \quad (\text{A3})$$

We note that the t dependence of the short-range $\delta(\mathbf{r})$ was integrated by Gauss–Legendre quadrature.

2. Momentum integrals

In this subsection, we draft the integration of the angular degrees of freedom in the momentum density, which is used in the second step of Eq. (26),

$$\int d\mathbf{p}_1 p_1^k \bar{\rho}(\mathbf{p}_1) = 4\pi \int_0^{\infty} dp p^{k+2} \bar{\rho}(p). \quad (\text{A4})$$

To work out this step, we write down the integral for two basis functions in Fourier space that is proportional to

$$\begin{aligned} \int d\mathbf{p}_1 p^k \exp(-ap_1^2 + \mathbf{d}^T \mathbf{p}_1) &= \int_0^{2\pi} d\phi \int_0^{\infty} dp p^{2+k} \int_0^{\pi} d\theta \sin \theta \exp(-ap^2 + i|\mathbf{d}|p \cos \theta) \\ &= 2\pi \int_0^{\infty} dp p^{k+2} \int_{-1}^1 dz \exp(-ap^2 + idpz) \\ &= \frac{4\pi}{d} \int_0^{\infty} dp p^{k+1} \sin(dp) e^{-ap^2}. \end{aligned} \quad (\text{A5})$$

We note that \mathbf{d} is purely imaginary for any configuration-space shift vectors, $\mathbf{s} \in \mathbb{R}^{3n}$, due to Eq. (25). The short-range part of the integral in Eq. (A5) can be calculated analytically which we show for $k = 2$:

$$\begin{aligned}
\langle p^2 \rangle_\Lambda &= \frac{4\pi}{d} \int_0^\Lambda dp p^3 e^{-ap^2} \sin(dp) = \frac{4\pi}{d} \partial_a \partial_d \int_0^\Lambda dp e^{-ap^2} \cos(dp) \\
&= \frac{4\pi}{2d} \partial_a \partial_d \int_0^\Lambda dp \left[e^{-ap^2+idp} + e^{-ap^2-idp} \right] \\
&= \frac{\pi^{3/2}}{d\sqrt{a}} \partial_a \partial_d e^{-\frac{d^2}{4a}} \left[\operatorname{erf} \left(\sqrt{a}\Lambda + \frac{id}{2\sqrt{a}} \right) + \operatorname{erf} \left(\sqrt{a}\Lambda - \frac{id}{2\sqrt{a}} \right) \right] \\
&= \frac{1}{8a^{7/2}d} \left\{ d(6a - d^2)\pi^{3/2} e^{-\frac{d^2}{4a}} \left[\operatorname{erf} \left(\sqrt{a}\Lambda + \frac{id}{2\sqrt{a}} \right) + \operatorname{erf} \left(\sqrt{a}\Lambda - \frac{id}{2\sqrt{a}} \right) \right] \right. \\
&\quad \left. - 4\pi\sqrt{a}e^{-a\Lambda^2} [2ad\Lambda \cos(d\Lambda) + (4a + 4a^2\Lambda^2 - d^2) \sin(d\Lambda)] \right\}. \tag{A6}
\end{aligned}$$

If ECGs are centered at the origin of the coordinate system, we need to consider the $d \rightarrow 0$ limit of the general expression:

$$\lim_{d \rightarrow 0} \langle p^2 \rangle_\Lambda = \frac{3\pi^{3/2}}{2a^{5/2}} \operatorname{erf}(\sqrt{a}\Lambda) - \frac{\pi\Lambda}{a^2} (3 + 2a\Lambda^2) e^{-a\Lambda^2}. \tag{A7}$$

Appendix B: Connection between wave function derivatives in real space and the decay rate of the asymptotic tail in momentum space

Let us consider an L^2 integrable function, $f(x)$, which decays to zero for $x \rightarrow \pm\infty$. Moreover, its $(k-1)$ th derivative is discontinuous at x_0 , and its k th derivative at this point is related to the Dirac delta function [34]

$$\frac{d^k f(x)}{dx^k} \sim \delta(x - x_0)A(x), \tag{B1}$$

where $A(x)$ is a continuous regular function, which describes the k th derivative everywhere else. Next, let us consider the Fourier transform of $f(x)$ and its momentum-space properties,

$$\tilde{f}(p) = \frac{1}{\sqrt{2\pi}} \int_{-\infty}^{\infty} dx f(x) e^{-ipx}. \tag{B2}$$

Using partial integration, $\tilde{f}(p)$ can be expressed with the integral of the derivative of $f(x)$,

$$\tilde{f}(p) = -\frac{1}{\sqrt{2\pi}ip} \underbrace{[f(x)e^{-ipx}]_{-\infty}^{\infty}}_0 + \frac{1}{\sqrt{2\pi}ip} \int_{-\infty}^{\infty} dx \frac{df(x)}{dx} e^{-ipx}, \tag{B3}$$

where the first term in the right hand is zero, since our original condition was $\lim_{x \rightarrow \pm\infty} f(x) = 0$. The partial integration can be repeated k times,

$$\tilde{f}(p) = \frac{1}{\sqrt{2\pi}} \int_{-\infty}^{\infty} dx f(x) e^{-ipx} = \frac{1}{\sqrt{2\pi}} \left(\frac{-i}{p} \right)^k \int_{-\infty}^{\infty} dx \frac{d^k f(x)}{dx^k} e^{-ipx} = \frac{1}{\sqrt{2\pi}} \left(\frac{-i}{p} \right)^k e^{-ipx_0} A(x_0), \tag{B4}$$

where Eq. (B1) is used and we assumed that the Dirac delta function predominantly determines the integral expression above. Since e^{-ipx_0} is bounded,

$$|e^{-ipx_0}| = 1, \tag{B5}$$

in the limit of large p values, $\tilde{f}(p)$ decays polynomially,

$$p > p_\Lambda : \quad \tilde{f}(p) \sim \frac{1}{p^k}. \tag{B6}$$

Appendix C: Fourier transformation of $rf(\vartheta, \varphi)$

In this section, we show that the Fourier transform of $rf(\vartheta, \varphi)$ is local, moreover, its contribution is zero in the asymptotic tail of the kinetic and mass-velocity term integrands. The function $f(\vartheta, \varphi)$ in Eq. (32) can be written as a linear combination of Y_{1m} spherical symmetric functions where the angular momentum quantum number is set to one. So, it is sufficient to consider $rY_{1m}(\vartheta, \varphi)$,

$$h(\mathbf{p}) = \frac{1}{\sqrt{8\pi^3}} \int d\mathbf{p} e^{i\mathbf{p}\mathbf{r}} rY_{1m}(\vartheta, \varphi) . \quad (\text{C1})$$

In order to perform the Fourier transformation let us expand the plane wave in terms of spherical harmonics [35],

$$e^{i\mathbf{p}\mathbf{r}} = 4\pi \sum_{\ell=0}^{\infty} \sum_{m=-\ell}^{\ell} i^{\ell} j_{\ell}(pr) Y_{\ell m}^* \left(\frac{\mathbf{p}}{p} \right) Y_{\ell m} \left(\frac{\mathbf{r}}{r} \right) , \quad (\text{C2})$$

where $j_{\ell}(x)$ is the spherical Bessel function [36]. Substituting back Eq. (C2) into Eq. (C1) and using the orthogonality relation between the spherical harmonics, the integral can be calculated for the angles,

$$h(\mathbf{p}) = \frac{i}{\sqrt{2\pi}} Y_{1m}^* \left(\frac{\mathbf{p}}{p} \right) \int dr r^3 j_1(pr) . \quad (\text{C3})$$

Using the following identity,

$$\frac{\partial}{\partial p} j_0(pr) = -r j_1(pr) , \quad (\text{C4})$$

we can rewrite the integral in Eq. (C3) as

$$h(\mathbf{p}) = -\frac{i}{\sqrt{2\pi}} Y_{1m}^* \left(\frac{\mathbf{p}}{p} \right) \frac{\partial}{\partial p} \int dr r^2 j_0(pr) . \quad (\text{C5})$$

Then, we can recognize one of the identities of the Dirac delta function [37], $\delta(p) = \frac{2p^2}{\pi} \int dr r^2 j_0(pr)$,

$$h(\mathbf{p}) = -\frac{\sqrt{2i}}{\pi^{3/2}} Y_{1m}^* \left(\frac{\mathbf{p}}{p} \right) \frac{\partial}{\partial p} \frac{\delta(p)}{p^2} , \quad (\text{C6})$$

and the differentiation can be performed by using the identity $\delta(x) = -x\delta'(x)$ for the derivative of the Dirac delta function,

$$h(\mathbf{p}) = \frac{3\sqrt{2i}}{\pi^{3/2}} \frac{\delta(p)}{p^3} Y_{1m}^* \left(\frac{\mathbf{p}}{p} \right) . \quad (\text{C7})$$

Due to $\delta(p)$, the obtained function is local, and thus, it does not contribute to the large p asymptotic tail.

Appendix D: Determination of the $\rho(0)$ and $\eta(0)$ values for the grounds state of the He atom

In order to determine accurate values for $\rho(0)$ and $\eta(0)$, the expectation values of $\delta(\mathbf{r}_{iA})$ and $\delta(\mathbf{r}_{ij})$ are obtained in an iterative procedure (Sec. II). The grid points used in the fitting are selected according to Sec. VI. For $\delta(\mathbf{r}_{iA})$ and $\delta(\mathbf{r}_{ij})$ the fitting intervals start at 5 bohr⁻¹, and at 1 bohr⁻¹, respectively, which are sufficient to avoid complicated correlation effects at low t values (see also Fig. 1). For the asymptotic range, the relative deviation of the integrands from the leading-order analytic terms is shown in Figure 5. The function $\mathcal{I}_{\delta(\mathbf{r}_{iA})}$ appears to be robust with respect to the number of basis functions, while $\mathcal{I}_{\delta(\mathbf{r}_{ij})}$ is more sensitive to the basis set.

After inspection of these figures, we set $t_{\Lambda} = 100$ bohr⁻¹ for the upper end of the interval used for the fitting, and the beginning of the long-range integral. The $\rho(0)$ and $\eta(0)$ values obtained in this computational setup with seven fitting parameters are collected in Table III.

Figure. 6 shows the relative error of $\langle\langle \delta(\mathbf{r}_{iA}) \rangle\rangle$ and $\langle\langle \delta(\mathbf{r}_{ij}) \rangle\rangle$ in comparison with data available from Ref. [2].

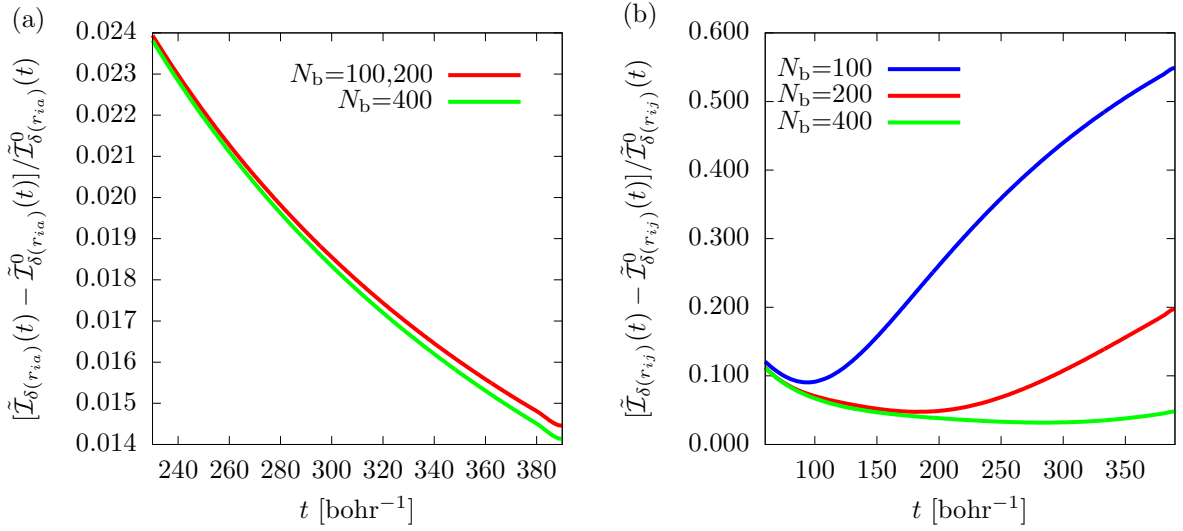


Figure 5. Relative difference in the asymptotic tail of the numerically calculated functions, $\mathcal{I}_{\delta(r_{ia})}(t)$ and $\mathcal{I}_{\delta(r_{ij})}(t)$, and the analytic leading order expressions of the asymptotic tail, $\tilde{\mathcal{I}}_{\delta(r_{ia})}^0(t) = 8\rho(0)/(\sqrt{\pi}t^2)$ and $\tilde{\mathcal{I}}_{\delta(r_{ij})}^0(t) = -2\eta(0)/(\sqrt{\pi}t^2)$ for the example of the ground state of the helium atom with an increasing number of ECG basis functions (N_b).

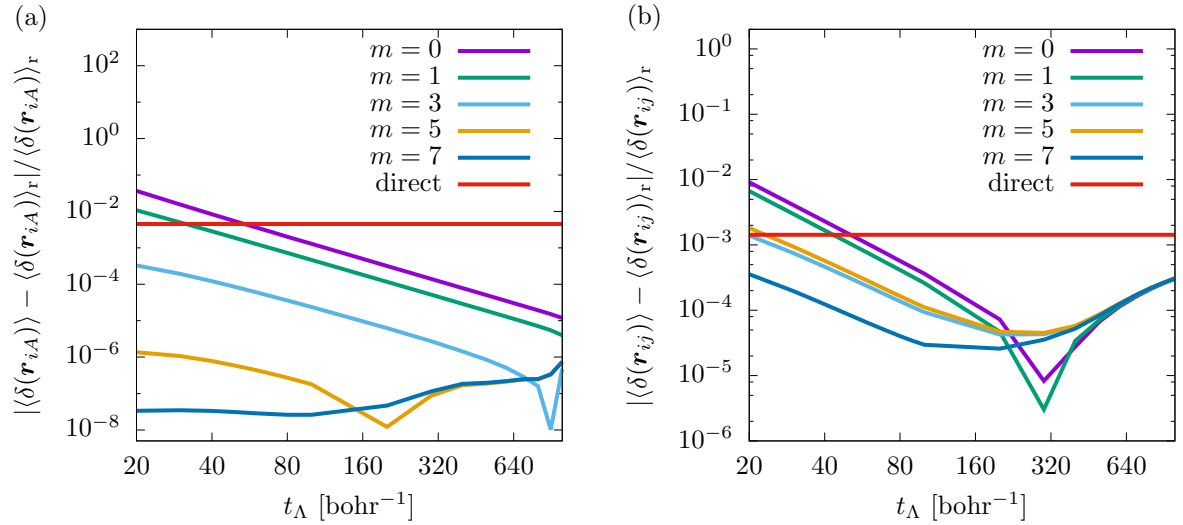


Figure 6. The relative error of $\langle \delta(r_{ia}) \rangle$ and $\langle \delta(r_{ij}) \rangle$ for various t threshold values and m number of fitting parameters, Eq. (20), using 400 ECGs. The result ‘direct’ was obtained by numerical integration using ECGs. $\langle \delta(r_{ia}) \rangle_r = 3.6208586377(3)$ bohr⁻¹ and $\langle \delta(r_{ij}) \rangle_r = 0.106345370636(2)$ bohr⁻¹ [2].

Table III. Convergence of the density and the pair-density functions at the coalescence point, in bohr⁻¹, with respect to the number of basis functions (N_b). $t = 100$ bohr⁻¹.

N_b	$\rho(0)$	$\eta(0)$
100	3.620 845 647	0.106 366 877
200	3.620 857 171	0.106 350 118
400	3.620 858 545	0.106 348 521
Ref. [2]	3.620 858 637 7(3)	0.106 345 370 636 (2)